Molecular dynamics study of liquid water under high compression*

Frank H. Stillinger

Bell Laboratories, Murray Hill, New Jersey 07974

Aneesur Rahman

Argonne National Laboratories, Argonne, Illinois 60439
(Received 18 July 1974)

The technique of computer simulation by molecular dynamics has been used to investigate highly compressed water at mass density 1.346 g/cm^3. The calculations involve 216 rigid molecules, subject to an additive interaction (the "ST2 potential") whose strong anisotropic character has been shown to describe the hydrogen bond phenomenon. In the light of previous calculations on the same model at ordinary pressures, substantial restructuring of the liquid in response to compression is obvious. No evidence arises to support description of the liquid in terms of crystal structures of ices VI and VII, the solid forms that might be expected to be relevant at the chosen density. The calculations indicate that the initial effect of pressure increase (at 1 atm) leads to increased fluidity, as is known to be the case for real water.

I. INTRODUCTION

The task of interpreting diverse experiments on water and its solutions in molecular terms has proved generally to be formidable. The richness of unusual phenomena has frequently led to a multiplicity of "models" or "pictures" which often stand in mutual contradiction.[1,2] With such severe problems of interpretive ambiguity, first-principles theory of liquid water becomes a particularly important potential source of unbiased insight.

In an effort to satisfy the need for a detailed and accurate molecular description of water, we have recently developed a moderately realistic simulation technique employing the computer-oriented method of "molecular dynamics." In this technique, one solves classical equations of motion numerically for a set of rigid water molecules, subject to additive interactions. The resulting chronological evolution of the mechanical system is recorded and used to calculate various statistical and dynamical averages of interest.

Following our initial feasibility study,[3] we have employed the molecular dynamics method to examine a variety of structural and kinetic properties for pure water, including the effects of temperature change.[4–6] The specific goal in this paper is the application of the molecular dynamics method to an analogous study of pressure effects in water.

It should be emphasized that the molecular dynamics approach possesses an inherent power far surpassing its capacity to explain available experiments. States of matter with experimentally unattainable conditions of temperature and pressure can be simulated as easily as states ordinarily encountered in the laboratory. Furthermore, there are many types of quantitative results (such as hydrogen bond polygon distributions)[6] which can be extracted from the molecular dynamics computations, for which no experiment can be devised.

Liquid water exhibits a variety of interesting pressure effects that ultimately require explanation in statistical-mechanical terms. Prominent among these are the following:

(a) suppression of the negative thermal expansion that causes the 4 °C density maximum at 1 bar[7];

(b) reduction in the temperature range (0 °C to 46 °C at 1 bar) over which the isothermal compressibility decreases with increasing temperatures[7];

(c) initial decrease of shear viscosity with increasing pressure (below 30 °C) followed by an increase at high pressure[8];

(d) increase in electrolyte conductance[9];

(e) initial increase in the proton spin–lattice relaxation time, with pressure, at low temperature.[10]

These effects furthermore have to be rationalized in a way that is consistent with the small variation with pressure of Raman band shapes that have been observed to 10 kbar.[11]

Although the present investigation has not been directed specifically toward each of the cited pressure effects, we believe that it bears on all of them indirectly. The high-pressure results reported here provide only a crude first glimpse at an area that ultimately needs to be examined with great care. Nevertheless, we hope that the limited information offered in this paper will help to understand the way in which real water responds to increasing pressure.

II. THERMODYNAMIC STATES

The additive molecular interaction upon which the present calculations are based, denoted for simplicity as the "ST2 potential," employs a four-point-charge model for each water molecule. This potential was designed specifically to describe the strong anisotropic interactions between neighboring molecules which produce hydrogen bonding, as well as to describe the dipole–dipole interactions which operate at large intermolecular separation. The interested reader should check Ref. 5 for a detailed specification of the ST2

potential and for a compilation of molecular dynamics results based upon that potential for the low pressure states with mass density $1\,g/cm^3$.

As was the case in the earlier work, we have used 216 water molecules confined to a cubical "unit cell." Periodic boundary conditions apply, so that the unit cell is surrounded by replicas of itself on all sides; thus, no real boundaries exist to affect the calculation of bulk properties adversely.

The liquid density is controlled by choice of L, the unit cell edge length. For the present investigation,

$$L = 16.86\ \text{Å}\ . \tag{II.1}$$

This corresponds to mass density

$$\rho = 1.346\,g/cm^3, \tag{II.2}$$

which we infer from Bridgeman's measurements[12] to be that appropriate to the experimental ice VI–ice VII–liquid triple point at[13]

$$p = 22.0\ \text{kbar},$$
$$T = 81.6\ ^\circ\text{C}. \tag{II.3}$$

This density selection was motivated in part by the desire to induce substantial shifts in computed quantities relative to the corresponding values at $1\,g/cm^3$. Furthermore, the known crystal structures of ice VI and ice VII provide natural points of comparison for the structure of the compressed liquid, in the same way that hexagonal ice I does for ordinary liquid water.

In order to speed up running times for the molecular dynamics program, we have followed the standard procedure of neglecting molecular interactions beyond a fixed cutoff distance R_c.[14] For the present series of calculations,

$$R_c = 7.6986\ \text{Å}\ . \tag{II.4}$$

Within this cutoff sphere, each molecule interacts with an average of about 85 other molecules.

Three distinct temperatures have been studied at the density shown in Eq. (II.2). They are listed in Table I. Each of these three dynamical runs spans about 2.1 psec. State "A" has sufficiently low temperature that it must be regarded as a supercooled liquid [see Eq. (II.3)]; if the experimental phase diagram is relevant to our model, then in a much longer dynamical run this state should freeze to ice VI.

Table I also provides some calculated thermodynamic properties for the three high-compression states. The energy per molecule E/N remains substantially unchanged during each run, and includes rotational and translational kinetic energy, as well as interactions out to R_c. The dimensionless pressure quantity $(p/\rho kT) - 1$ was evaluated through the average virial of intermolecular forces (again neglecting forces beyond R_c). The isothermal compressibility κ_T, in the dimensionless combination $\rho kT\kappa_T$, was evaluated from long-wavelength collective density fluctuations within the system. Finally, Table I includes mean-square values $\langle M^2 \rangle$ for the vector sum M of unit vectors for the individual molecule dipole moment directions.

TABLE I. High-compression thermodynamic states for which liquid water has been studied in the present investigation.

State	A	B	C
Temperature (°C)	57	97	148
$\frac{p}{\rho kT} - 1$	3.7	3.9	4.0
$\rho kT\kappa_T$	0.032	0.034	0.044
E/N (kcal/mole)	−7.954	−7.196	−6.439
$\langle M^2 \rangle / N$	0.14	0.157	0.16

The entries in Table I show that the increased density has been accompanied by a substantial increase in pressure; but the increase is significantly smaller than the amount required by experiment. Combining data in Eqs. (II.2) and (II.3), for example, one finds

$$(p/\rho kT) - 1 = 8.98 \tag{II.5}$$

at the ice VI–ice VII–liquid triple point. We believe that our model calculations fall well below this value due partly to their neglect of potential nonadditivity in water, as well as to the neglect of quantum corrections. Nevertheless, we suggest that the major structural shifts exhibited by our calculations are still relevant, for they represent (as in real water) a competition between the tendency of strongly directional forces to build an open hydrogen-bond network, and the tendency for external pressure to force molecules into an efficient packing scheme.

The isothermal compressibilities listed in Table I are lower, by roughly a factor 5, than Ref. 5 indicates for the model at $1\,g/cm^3$ and corresponding temperatures. This marked decrease is consistent with Bridgman's equation of state measurements.[12]

Again by comparing with Ref. 5, it can be verified that isothermal compression from $1\,g/cm^3$ to $1.346\,g/cm^3$ reduces $\langle M^2 \rangle / N$ by amount 0.02 at all temperatures studied. Increasing the density has therefore enhanced the tendency for randomly selected pairs of molecules to point their dipoles in opposite directions.

From Table I we can infer that the constant-volume heat capacity C_V is about 17 cal/mole · deg for the ST2 model at $1.346\,g/cm^3$, and 97 °C, with indications that it declines with increasing temperature. This magnitude should be compared with the larger C_V that obtains for the model at the same temperature but $1\,g/cm^3$, namely 25 cal/mole · deg. The implication is that compression inhibits thermally induced restructuring of the liquid.

Since the molecular dynamics method follows the chronological evolution of the system, it is possible to evaluate the self-diffusion constant D. By monitoring mean-square displacements of molecular centers of mass, we infer that

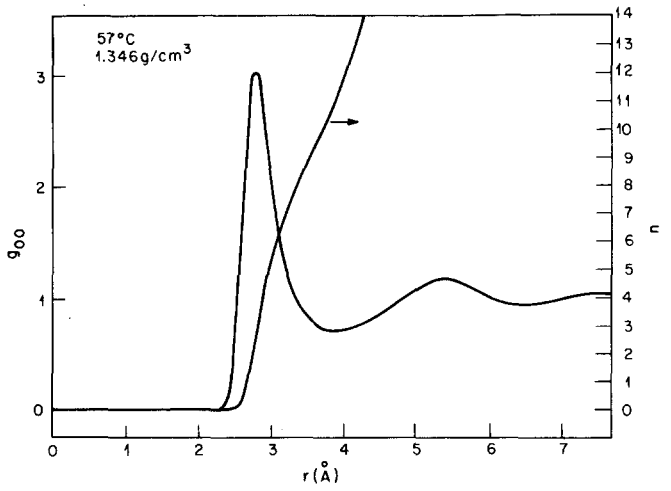

FIG. 1. Pair correlation function $g_{00}(r)$ and associated running coordination number $n(r)$ for liquid water at 57 °C and 1.346 g/cm^3.

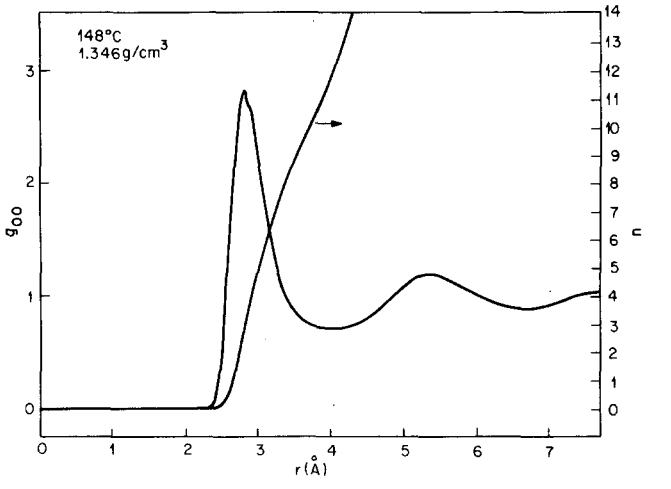

FIG. 3. Pair correlation function and running coordination number for liquid water at 148 °C and 1.346 g/cm^3.

$$D \cong 6.5 \times 10^{-5} \text{ cm}^2/\text{sec} \qquad \text{(II.6)}$$

for run "B" at 1.346 g/cm^3 and 97 °C. This is only slightly below the interpolated value

$$D \cong 7.2 \times 10^{-5} \text{ cm}^2/\text{sec} \qquad \text{(II.7)}$$

implied for 97 °C by previous ST2 calculations at 1 g/cm^3. This remarkable similarity of D values in spite of 35% density increase will be discussed in Sec. VI.

III. OXYGEN PAIR DISTRIBUTIONS

The distribution of pair distances between oxygen nuclei in the liquid can be represented in terms of the pair correlation function $g_{00}(r)$. It is conventional to normalize this function to unity for large distance r. Figures 1–3 report the correlation functions g_{00} calculated for the three states investigated. The figures also include running coordination numbers

$$n(r) = 4\pi (N/V) \int_0^r r^2 g_{00}(r)\, dr. \qquad \text{(III.1)}$$

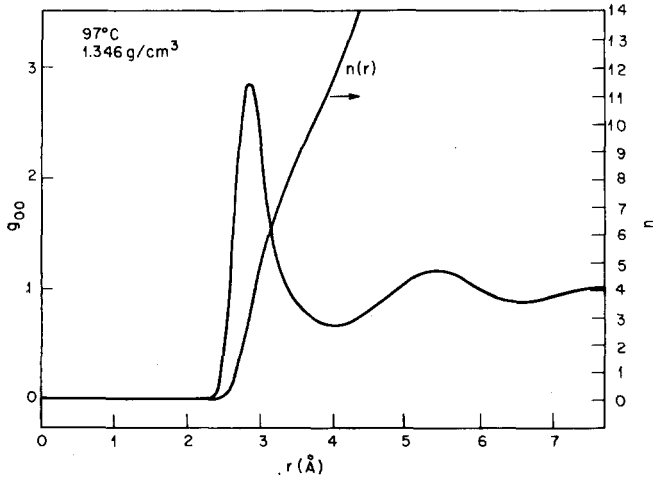

FIG. 2. Pair correlation function and running coordination number for liquid water at 97 °C and 1.346 g/cm^3.

In broad terms, the functions shown in the figures resemble those previously computed for 1 g/cm^3, but there are important differences of quantitative detail:

(a) The maximum corresponding to the first-neighbor shell occurs about 0.03 Å closer to the origin than it does at low pressure, reflecting a small degree of hydrogen-bond compression. (Note, however, that this maximum would move 0.27 Å inward if the 35% density increase produced isotropic shrinkage of the intermolecular structure.)

(b) The second maximum for all three high-pressure states occurs at about 1.9 times the distance at which the first peak occurs. In the low-pressure liquid, the corresponding distance ratio is close to the value 1.633 that results from ideal tetrahedral bonding (as in ice Ih). The intervening minimum between the first and second maxima has also shifted to larger distance as a result of the compression. Due to these shifts, the high-pressure correlation functions tend more to resemble those for "simple" liquids (such as argon).

(c) Especially beyond the first maximum, the damped oscillations of $g_{00}(r)$ about unity have noticeably greater amplitudes (at a given temperature) in the compressed state than they do at low pressure.

(d) If the number of "nearest neighbors" is identified as the value of the running coordination number $n(r)$ at the first $g_{00}(r)$ minimum, one finds from Fig. 1–3 at 57°, 97°, and 148° that there are 10.8, 11.7, and 11.8 neighbors, respectively. These numbers are about twice those found at low pressure,[5] and clearly signify major structural changes in response to high compression. Even if the somewhat smaller distances for the low-pressure $g_{00}(r)$ minima were employed, one would still find 9–10 nearest neighbors in the compressed liquid. Consistent with (b) above, $n(r)$ also implies packing characteristics very similar to those in monatomic liquids.

The crystal structures of ice VI and ice VII display, respectively, four and eight nearest neighbors for each

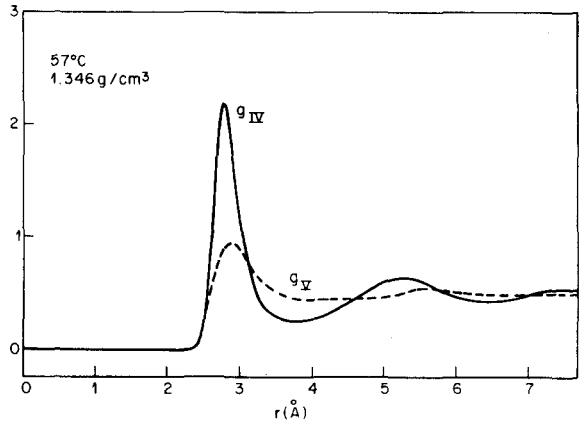

FIG. 4. Octahedrally resolved components of the oxygen–oxygen correlation function at 57 °C, 1.346 g/cm^3. First neighbors connected by undistorted linear hydrogen bonds appear exclusively in g_{IV}.

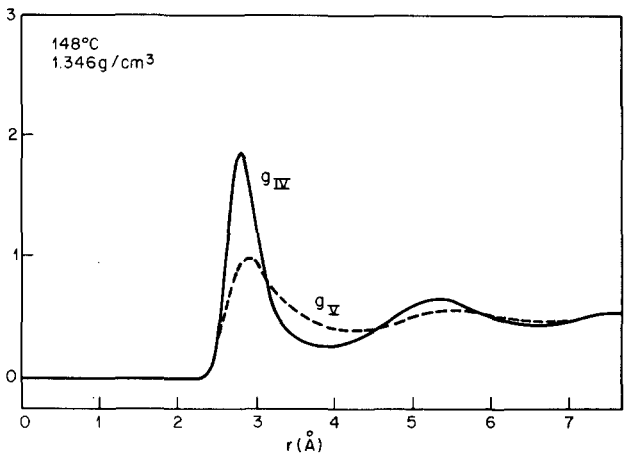

FIG. 6. Octahedral components of the oxygen–oxygen pair correlation function at 148 °C, 1.346 g/cm^3.

molecule at a sharply defined distance (2.81 Å for ice VI, 2.86 Å for ice VII.[15] Since a volume increase accompanies the melting of both of these ices, it is not possible to rationalize the larger number of nearest neighbors in the liquid in terms of "interstitial" molecules in an otherwise slightly disordered ice structure. Furthermore, no obvious large cavities are present in either the ice VI or ice VII structures (analogous to those in ices Ih and Ic) to accommodate interstitials easily.

If substantial numbers of ice VI or ice VII fragments were present in the liquid, their existence might be revealed in $g_{00}(r)$ by occurrence of pair distances corresponding to characteristic second, third, ..., neighbor separations in the respective crystals. In ice VI, eight nonbonded neighbors occur at 3.51 Å; six nonbonded neighbors occur at 3.30 Å in ice VII. Neither of these distances is prominently distinguished in Fig. 1–3. We conclude that if these fragments are present in significant concentration, they have been camouflaged by large distortions.

Increasing the temperature causes a slight reduction in the height of the $g_{00}(r)$ first peak for the density 1.346 g/cm^3. However, it should be stressed that considerably less sensitivity to temperature is involved compared to the prior observations[5] at 1 g/cm^3. In fact, the $g_{00}(r)$ curves for 97 °C (Fig. 2) and 148 °C (Fig. 3) are nearly indistinguishable, within statistical uncertainty.

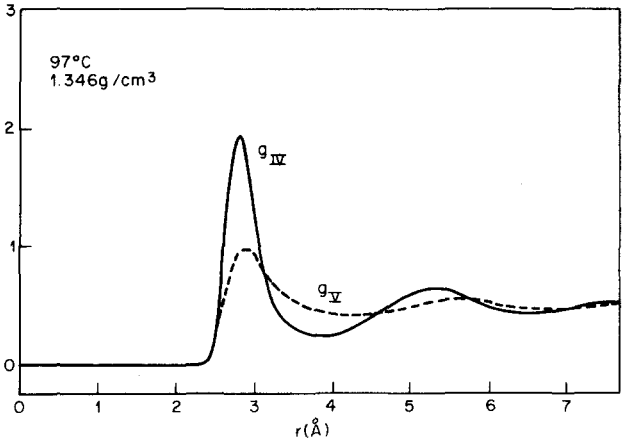

FIG. 5. Octahedral components of the oxygen–oxygen pair correlation function, for 97 °C, 1.346 g/cm^3.

We have previously found that it is profitable to analyze the functions $g_{00}(r)$ into distinct angular components that correspond to faces of a regular polyhedron.[3,4] In the case of an octahedral resolution, we write

$$g_{00}(r) = g_{IV}(r) + g_V(r) , \qquad \text{(III.2)}$$

following the established notation. Here, one water has been surrounded by a regular octahedron centered on the oxygen nucleus. The octahedron has been oriented so that the molecule's four fundamental tetrahedral directions (two OH bonds, and two directions from O to negative point charges) simultaneously pierce the centers of four nonadjacent octahedron faces. These faces are designated "IV," and the remaining four faces are designated "V." The component functions $g_{IV}(r)$ and $g_V(r)$ comprise neighbor oxygens residing in the respective portions of the full direction space.

The value of the octahedral resolution lies largely in its relation to the ideal tetrahedrally bonded networks of ices Ih, Ic, and VII. With each of these three structures, the four nearest-neighbor oxygens that are connected to the central one by linear hydrogen bonds would appear only in $g_{IV}(r)$. For ices Ih and Ic, this exhausts the first neighbors, and $g_V(r)$ would be zero at the first-neighbor distance. However, with ice VII, the four nonbonded first neighbors occur in $g_V(r)$.

The angular apertures of the class IV and class V faces are sufficiently large that even with the distortion from ideal tetrahedral directions displayed by hydrogen bonds in ice VI, its four bonded nearest neighbors would appear exclusively in $g_{IV}(r)$.

Figures 4–6 show the pairs of functions g_{IV} and g_V for the three temperatures. They clearly demonstrate

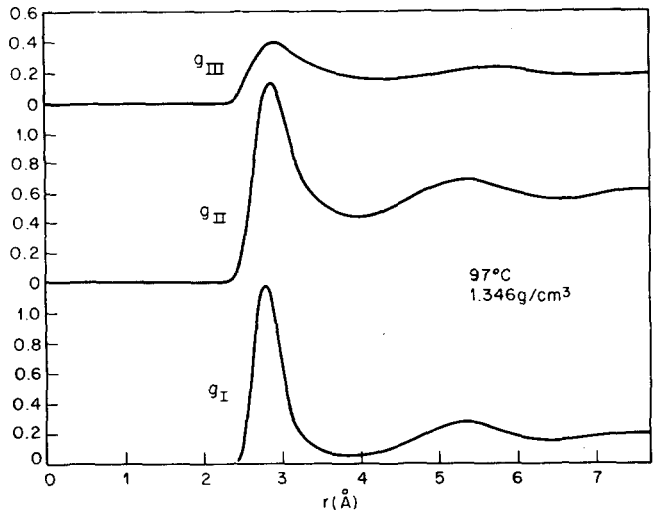

FIG. 7. Icosahedral components of $g_{00}(r)$ for liquid water at 97 °C and 1.346 g/cm^3.

the angular inhomogeneity of matter distribution in the vicinity of a molecule with specified orientation. As might have been expected, first neighbors in region IV are spatially more localized than those in region V, doubtless owing to the strong hydrogen bonds that form in region IV. Evidently this first-neighbor localization is the principal reason that succeeding damped oscillations in $g_{IV}(r)$ have considerably greater amplitude (i.e., greater localization) than those in $g_V(r)$.

At low pressure, most first neighbors appear in $g_{IV}(r)$.[4] But in the present case, roughly equal numbers of first neighbors occur in the two regions. Those in region V have been forced into place by packing considerations at high pressure, and it is significant that the first maximum of $g_V(r)$ at all three temperatures examined lies 0.12 Å farther from the origin than the first $g_{IV}(r)$ maximum.

As in the case of $g_{00}(r)$, the separate octahedral components are rather insensitive to temperature change.

An icosahedral resolution of $g_{00}(r)$ can also be performed, giving three distinct angular components[3,4]:

$$g_{00}(r) = g_I(r) + g_{II}(r) + g_{III}(r) \ . \qquad \text{(III.3)}$$

On account of the greater number of polyhedron faces involved, this resolution tends to provide greater angular discrimination than the octahedral version. All tetrahedrally directed linear hydrogen bonds are comprised in $g_I(r)$; $g_{III}(r)$ corresponds to the four polyhedron faces directly opposite those of class I, and $g_{II}(r)$ collects pairs for the remaining twelve faces.

Our calculations show that the icosahedral components are rather resistant to temperature change, just as g_{00} and its octahedral components were found to be. The most visible temperature variation occurs as height reduction and broadening of the first g_I peak. At all temperatures, the distances to the first maxima increase in passing from g_I to g_{II} to g_{III}.

Figure 7 shows the three icosahedral components for 97 °C together. Pressure-induced packing changes, relative to ordinary pressure, are evident in g_{II} and g_{III} in the form of strongly enhanced peaks in the first-neighbor distance range.

IV. POTENTIAL ENERGY DISTRIBUTION FUNCTION

In a collection of N molecules interacting via additive pair interactions, each of the $\frac{1}{2}N(N-1)$ pairs possesses a value V of the pair potential which changes in times as the molecules move relative to one another. All pairs are equivalent at equilibrium, so the distribution of V values for any one pair must be identical to that for any other pair. We denote that distribution function by $P(V)$. Clearly, it will depend on the temperature and density prevailing in the system.

The absolute minimum for the ST2 potential used in the present series of calculations is $V_{min} = -6.839$ kcal/mole. Consequently, $P(V)$ would vanish identically for this model whenever V were below V_{min}.

If N were very large, the overwhelming majority of pairs would be widely separated, and thus weakly interacting. It is convenient to normalize $P(V)$ in the conventional large-system limit ($N \to \infty$, with density and temperature held fixed) so that for any $0 > V_0 > V_{min}$, $P(V_0)$ is independent of N. Then the infinite-system limit for P includes a second-order pole at $V = 0$.

Figure 8 shows the pair potential distributions that have been computed for the three high-compression states. Even though the system contains only $N = 216$ molecules, the strong tendency for $P(V)$ to concentrate most of its weight around $V = 0$ is obvious.

Distributions $P(V)$ have been previously computed via molecular dynamics for the ST2 model at 1 g/cm^3, in the temperature range -3 °C to 118 °C.[5] That range overlaps the present calculations sufficiently to permit identification of significant isothermal compression effects. Most striking perhaps is the removal of the nonmonotonic behavior of the low-pressure $P(V)$ for negative V, which produced a relative minimum near $V = -3$ kcal/mole for temperatures below about 100 °C. Although an obvious "shoulder" exists for each of the high-density $P(V)$ curves in Fig. 8, no maxima or minima occur at $V < 0$ for any temperature, even including the strongly undercooled regime.

The data presented in Fig. 8 indicate that $P(V)$ at 1.346 g/cm^3 is virtually independent of temperature at

$$V = -3.5 \text{ kcal/mole} \ . \qquad \text{(IV.1)}$$

This should be compared to the corresponding invariance point at -4.0 kcal/mole previously noted at 1 g/cm^3.

Over-all, the high-density distribution functions shown in Fig. 8 are considerably less sensitive to changes in temperature than their counterparts at 1 g/cm^3. This is consistent with, and reinforces, the similar observations already mentioned for the pair correlation functions. Furthermore, it supplies a detailed basis upon which to explain the previously noted reduction in C_V resulting from compression.

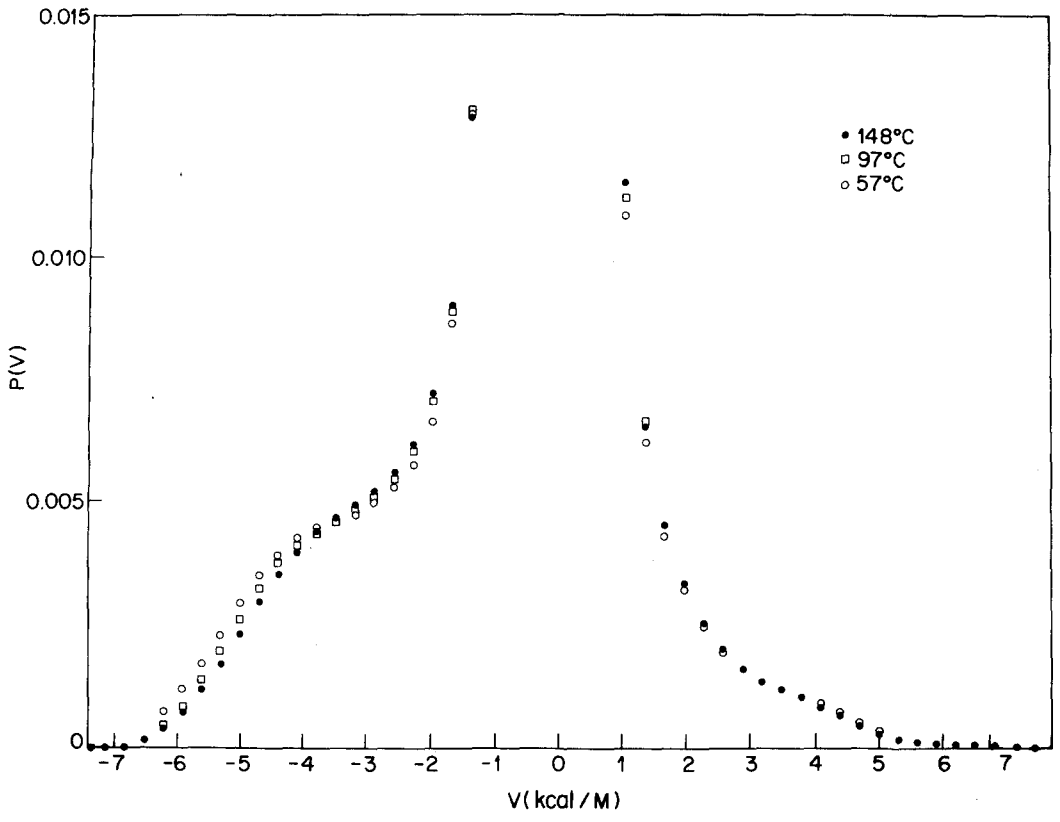

FIG. 8. Pair potential distribution functions for liquid water at 1.346 g/cm^3.

The shapes shown in Fig. 8 for $P(V)$ near $V=+4$ kcal/mole are unlike the low-pressure forms at any temperature. A weak but undeniable shoulder exists here. It presumably corresponds to the necessity of jamming particles into energetically unfavorable positions to satisfy the requirement of efficient use of available space. Were it not for this $V>0$ shape change, the effect of density increase on $P(V)$ would be quite similar to that of increasing the temperature strongly.

V. HYDROGEN BOND DISTRIBUTIONS

With the ST2 interaction, hydrogen bonding is associated with regions of relative configuration space for two molecules in which the potential is negative. These regions typically are rather restricted in distance and angles, and permit one to distinguish molecules according to their roles as "proton donor" or "proton acceptor." In order to classify molecular pairs unambiguously into those that are hydrogen bonded and those that are not, we have found it convenient to employ a "cutoff interaction magnitude" V_{HB}. Then if $V(i, j)$ represents the ST2 potential for molecules i and j in a given configuration, we use the convention

$$\begin{aligned} V(i, j) &\leq V_{HB}, \quad \text{(i, j hydrogen bonded)}, \\ V(i, j) &> V_{HB}, \quad \text{(i, j not hydrogen bonded)}. \end{aligned} \tag{V.1}$$

No uniquely qualified value can be identified for V_{HB} on physical or chemical grounds. Nevertheless, most phenomenological definitions would probably require V_{HB} to fall in the range -3 to -4 kcal/mole. For the present investigation, we have spanned a very wide range of possible V_{HB} choices, by employing the following set of ten magnitudes (j = 1, 2, ..., 10):

$$V_{HB}(j) = -0.6060\,(j-1) \text{ kcal/mole}. \tag{V.2}$$

Notice that the case j = 7 probably corresponds most closely to the conventional understanding of hydrogen bonding.

Figures 9–11 show the fractions of molecules, in our three high pressure runs, engaging simultaneously in 0, 1, 2, ... hydrogen bonds, with each of the ten alternative choices for V_{HB}. As j increases, the configurational requirements for formation of hydrogen bonds become increasingly more stringent, and it is obvious from the figures that the average number of hydrogen bonds per molecule declines.

Qualitatively, the histograms for hydrogen bond numbers in Fig. 9–11 are similar to those that have been presented before at low pressure.[4] At each of the three temperatures, the distributions are singly peaked, with mean values that decrease (at fixed j) as temperature increases. The failure for bimodal distributions to appear for any j allows us to extend to high pressure the former criticism of the interstitial models of liquid water,[3,4] which postulate a fully bonded network (each molecule with four bonds) invaded by unbonded guest molecules (no hydrogen bonds).

The predominant influence of compression on the hydrogen bond distributions appears for j = 2, 3, and 4. These choices for j count rather weak negative interactions as "hydrogen bonds." Increasing the density permits any one molecule to interact locally with more neighbors than otherwise, so the distributions are displaced to higher average numbers of hydrogen bonds. On the other hand, distributions for large j (7–10) are

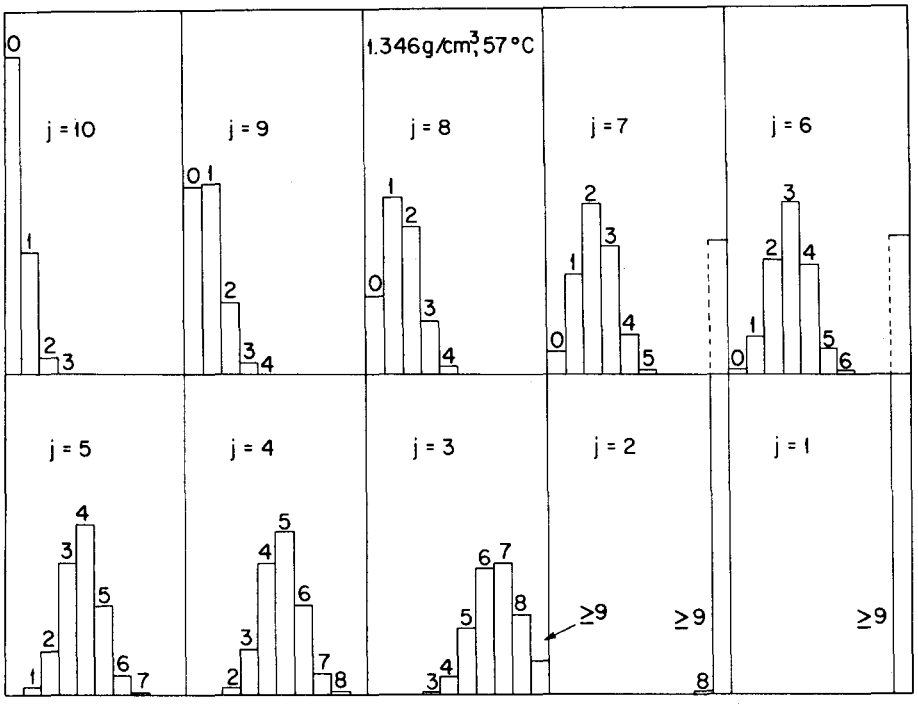

FIG. 9. Distributions of molecules at 57 °C, 1.346 g/cm^3, according to the number of hydrogen bonds in which they simultaneously participate. The alternative choices for cutoff interaction $V_{HB}(j)$ are provided by Eq. (V.2).

less sensitive to compression, since only four undistorted hydrogen bonds to any molecule are geometrically possible at any density.

VI. DISCUSSION

At low pressure, the best description of structure in liquid water as represented by the ST2 model seems to be that of a random and defective hydrogen-bond network.[5] The high directionality of the interactions gives rise to a rather open structure, an extreme form of which appears in ices Ih and Ic. In order for molecules to diffuse, hydrogen bond breakage is probably frequently necessary, and so the high value observed for the energy of activation for self-diffusion (about 4.5 kcal/mole[16]) makes sense.

Under high compression, such as that studied in this paper, the random network is forced to adopt more compact arrangements, in which mutual orientations play a less significant role. On the basis of results presented above, it appears that this compactness is associated with distortion of hydrogen-bond directions, and with mutual interpenetration of subsections of the random network. In the initial stages of compression, the former process seems likely to be the more predominant.

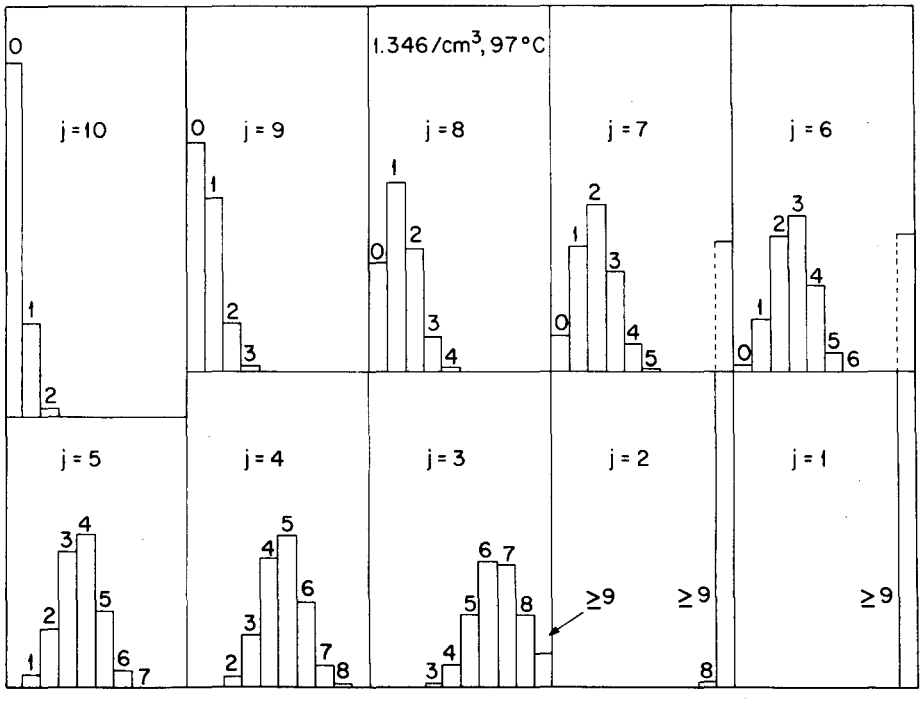

FIG. 10. Hydrogen-bond distributions for 97 °C, 1.346 g/cm^3.

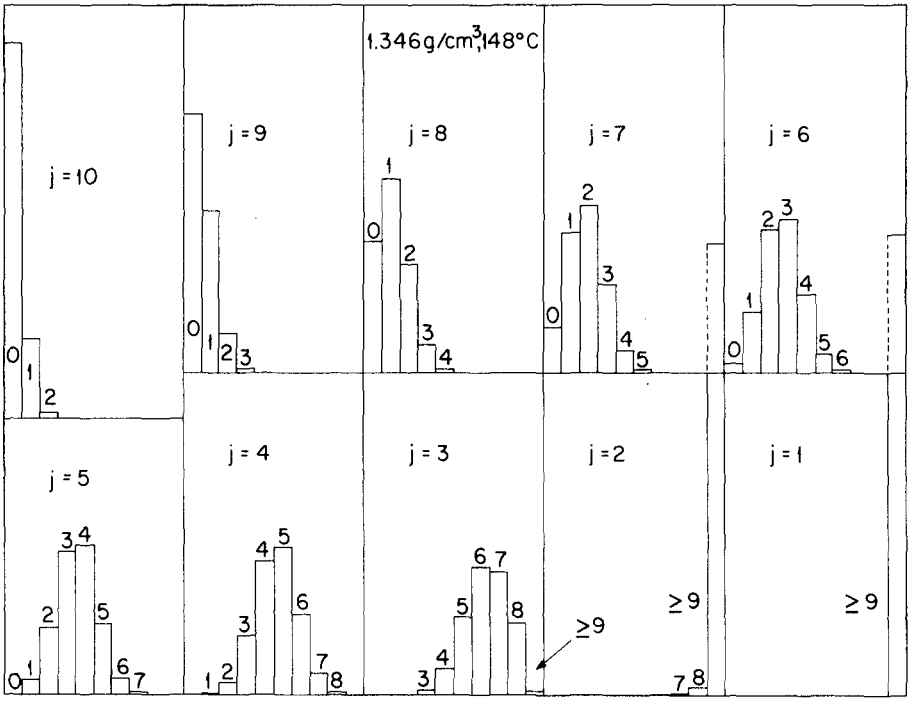

FIG. 11. Hydrogen-bond distributions for 148 °C, 1.346 g/cm^3.

If the mass density of a simple liquid like argon were increased by 35%, strong crowding together of the molecules would severely retard the self-diffusion process through mutual interference. By contrast, the mere 10% reduction in D shown by Eqs. (II. 6) and (II. 7) for the same density increase seems anomalously small.[17] Probably this comparison indicates that the present model for water is capable of explaining the tendency of real water to exhibit increased fluidity with initial pressure rise, as indicated by (c)–(e) in the Introduction.

This initial increase in fluidity with pressure can provisionally be explained in terms of the distorted hydrogen bonds produced by crushing the random network. It is easier to break an already distorted hydrogen bond than an undistorted one, as required by molecular diffusion or hydrodynamic shear flow. This picture suggests that the activation energies for self-diffusion and for viscosity should decline with increasing pressure. It will eventually be interesting to see if more extensive molecular dynamics calculation on the ST2 model will confirm that hypothesis quantitatively.

*Part of the work carried out at the Argonne National Laboratory was supported by the U. S. Atomic Energy Commission.

[1] *Water and Aqueous Solutions. Structure, Thermodynamics, and Transport Processes*, edited by R. A. Horne (Wiley-Interscience, New York, 1972). See, especially, Chaps. 9 and 10.
[2] A. Holtzer and M. F. Emerson, J. Phys. Chem. **73**, 26 (1969).
[3] A. Rahman and F. H. Stillinger, J. Chem. Phys. **55**, 3336 (1971).
[4] F. H. Stillinger and A. Rahman, J. Chem. Phys. **57**, 1281 (1972).
[5] F. H. Stillinger and A. Rahman, J. Chem. Phys. **60**, 1545 (1974).
[6] A. Rahman and F. H. Stillinger, J. Am. Chem. Soc. **95**, 7943 (1973).
[7] D. Eisenberg and W. Kauzmann, *The Structure and Properties of Water* (Oxford U. P., New York, 1969), p. 185.
[8] R. A. Horne and D. S. Johnson, J. Phys. Chem. **70**, 2182 (1966).
[9] Reference 1, Chap. 19.
[10] H. G. Hertz and C. Rädle, Z. Phys. Chem. (Frankf. a. M.) **68**, 324 (1969).
[11] G. E. Walrafen, J. Solution Chem. **2**, 159 (1973).
[12] P. W. Bridgman, Proc. Am. Acad. Arts Sci. **74**, 399 (1942).
[13] Reference 7, p. 93.
[14] In calculations involving water, it is the distance between oxygen nuclei which is relevant.
[15] Reference 7, pp. 87–9.
[16] Reference 7, p. 219.
[17] J. H. Dymond and B. J. Alder, J. Chem. Phys. **48**, 343 (1968).